Journal of Mines, Metals and Fuels, *73(8): 2515-2537; 2025. DOI: 10.18311/jmmf/2025/48211*

Print ISSN : 0022-2755

Journal of Mines, Metals and Fuels

Contents available at: *www.informaticsjournals.co.in/index.php/jmmf*

Influence of Mineral Composition and Microstructural Features on the Tensile Failure Mechanisms of Granite and Marble

Parveen Kumar, Srijan Srijan*, Vanita Aggarwal and Baljit Singh Walia

Department of Civil Engineering, Maharishi Markandeshwar Engineering College, Maharishi Markandeshwar (Deemed to be University), Mullana-Ambala - 133207, Haryana, India; srijanpurvey@gmail.com

Abstract

A comprehensive mineralogical analysis of granite and marble rocks was conducted using powder X-Ray Diffraction (XRD) and Scanning Electron Microscopy coupled with Energy-Dispersive Spectroscopy (SEM-EDS). The comparative evaluation of XRD and SEM-EDS data revealed a strong correlation, confirming the congruence of mineral compositions derived from both techniques. Detailed oxide composition analyses of Aswan red, light grey, and dark grey granite samples indicated a high degree of similarity, with trace elements such as C, O, Na, Al, K, and Ca uniformly dispersed within the silica matrix. The granite specimens were classified as peraluminous, predominantly composed of quartz, feldspar, and iron-aluminum oxides. In contrast, white marble samples, largely comprising carbonate minerals, exhibited distinct mineralogical characteristics. Mechanical testing using the Brazilian disc method has demonstrated that mineral composition significantly influences tensile strength. Because of its high SiO2 content and interconnecting crystalline structure, light grey granite has the maximum tensile strength, 1.45 MPa. Aswan red and dark grey granites showed similar mechanical reactions, according to their similar mineralogy, with tensile strengths of 1.42 MPa and 1.37 MPa, respectively. The composition of white marble, which contains dolomite and calcite, which are naturally less resistant to tensile failure, resulted in the lowest tensile strength of 0.89 MPa. The results confirm that feldspar and SiO2 minerals are essential for improving the mechanical integrity of granite. Conversely, the lower tensile strength of white marble is consistent with a softer mineralogical structure.

Major Findings: *Light grey granite has higher tensile strength than aswan red and dark grey granites because of high SiO2 content. White marble has the lowest tensile strength because of high calcium and magnesium content and soft mineralogical structure. Tensile strength data from the Brazilian disc method provides the insight of impact of mineral composition on mechanical properties.*

Keywords: *Granite, Marble, Structural and Mineralogical Analysis, Tensile Strength, XRD and SEM-EDS Techniques*

1.0 Introduction

Granite and marble are two most widely used rock materials in the construction and ornamental industries[1]. Both materials are well-known for their aesthetics, adaptability, and durability. Granite, an igneous rock mostly composed of quartz, feldspar, and mica, is noted for its high compressive strength, weather resistance, and durability, making it the most commonly used material in load-bearing applications[2]. Marble is a metamorphic rock formed by the re-crystallization of carbonate minerals, primarily calcite under high pressure and temperature. It is more prone to chemical weathering, particularly when exposed to acidic environments[3].

*Author for correspondence

Several mineralogical studies have been performed on various construction materials to determine their elemental and structural compositions[4–21]. Researchers employed X-Ray Diffraction (XRD) and Scanning Electron Microscopy with energy-dispersive spectroscopy (SEM-EDS) techniques to assess the mineralogical composition and microstructure of limestone, revealing that it is predominantly composed of calcite and dolomite. The presence of the calcite phase explains chemical weathering in stone, whereas traces of magnesium and iron influence the stone's deteriorating behaviour[22]. A comprehensive investigation of basalt, an extrusive igneous rock, revealed the presence of plagioclase and pyroxene, as well as traces of titanium, which accounts for its great mechanical strength and resistance to weathering[23]. A similar investigation on bentonite clay found montmorillonite to be the main mineral, as well as silicon, aluminium, and oxygen, which are responsible for clay swelling and adsorption capacity[24]. Researchers have also used XRD and SEM-EDS techniques to investigate the surface morphology and elemental composition of marble, describing its colour and durability properties[25]. Other than these, Other than these, several investigations have been undertaken using a variety of approaches to specify mineralogical features of different materials[26–37]. In the last decade numerous studies have been carried out on various materials such as limestone, basalt, fly ash, and geopolymer composites. Despite this, there is a significant gap in the comprehensive examination of marble and granite. Further research is required to fully comprehend the microstructural behaviour, elemental composition, and long-term durability of these stones under various environmental circumstances, as the majority of current research focuses on a particular facet of these material properties.

In addition, the mechanical properties of rocks are closely linked to their mineralogical composition and microstructural characteristics[38]. Several studies have established a positive correlation between quartz content and uniaxial compressive strength in granites and sandstones. However, the effect of mineral grain size on rock strength remains largely qualitative, with existing research indicating a general trend of negative correlation between grain size and both strength and brittleness.

This study addresses the research gap by conducting a thorough comparative investigation of commercially available granite and marble from four different places in India, employing sophisticated techniques including XRD, SEM-EDS, thin-section analysis, and Brazilian indirect tensile testing. The findings revealed that granite predominantly consists of silicon dioxide (SiO_2), aluminium oxide (Al_2O_3), and sodium erbium fluoride ($NaErF_4$), while marble is primarily composed of calcium carbonate ($CaCO_3$) and calcium magnesium carbonate ($CaMg(CO_3)_2$). Increased crystalline grain size in both materials was associated with higher mechanical strength[39].

Marble's mechanical strength and brittleness are significantly affected by changes in grain size, mineral content, and failure patterns, according to tensile tests. An integrated approach incorporating microstructural and mechanical investigations is essential for understanding the performance, durability, and failure processes of granite and marble under various environmental conditions.

2.0 Experimental Details

2.1 Materials and Instruments Utilised

In this study, four different types of samples of granite and marble stones were used. The type of the materials and their sourcing location are given in Table 1. Figure 1 illustrates polished portions of all four materials utilized in this investigation. X-Ray Diffraction (XRD) and Scanning Electron Microscopy with Energy-Dispersive Spectroscopy (SEM-EDS) were employed to quantitatively analyse the crystalline minerals in all samples.

Table 1. Various materials utilized in the study along with its source

S.No.	Material	Source
1.	Dark Grey Granite	Warangal, Telangana, India
2.	Ligh Grey Granite	Jalore, Rajasthan, India
3.	Aswan Red Granite	Krishnagiri, Tamil Nadu, India
4.	White Marble (Makrana Marble)	Makrana, Rajasthan, India

2.2 Sample Preparation

For mineral quantification, samples were collected from two tiles of each material to be analysed in the current study. The samples from each tile were grinded in compact jaw crusher and mixed in equal proportion to represent better morphological characteristics. The mixed sample powders were subjected to additional fine grinding by the help of agate mortar and pestle. Similar sample preparation technique has been followed by other researchers[40,41].

For tensile strength, the prepared samples were then cut into disc shapes using a diamond saw, ensuring precise geometry and smooth edges to minimize stress concentrations during testing as illustrated in Figure 2. The disc specimens were further polished to achieve

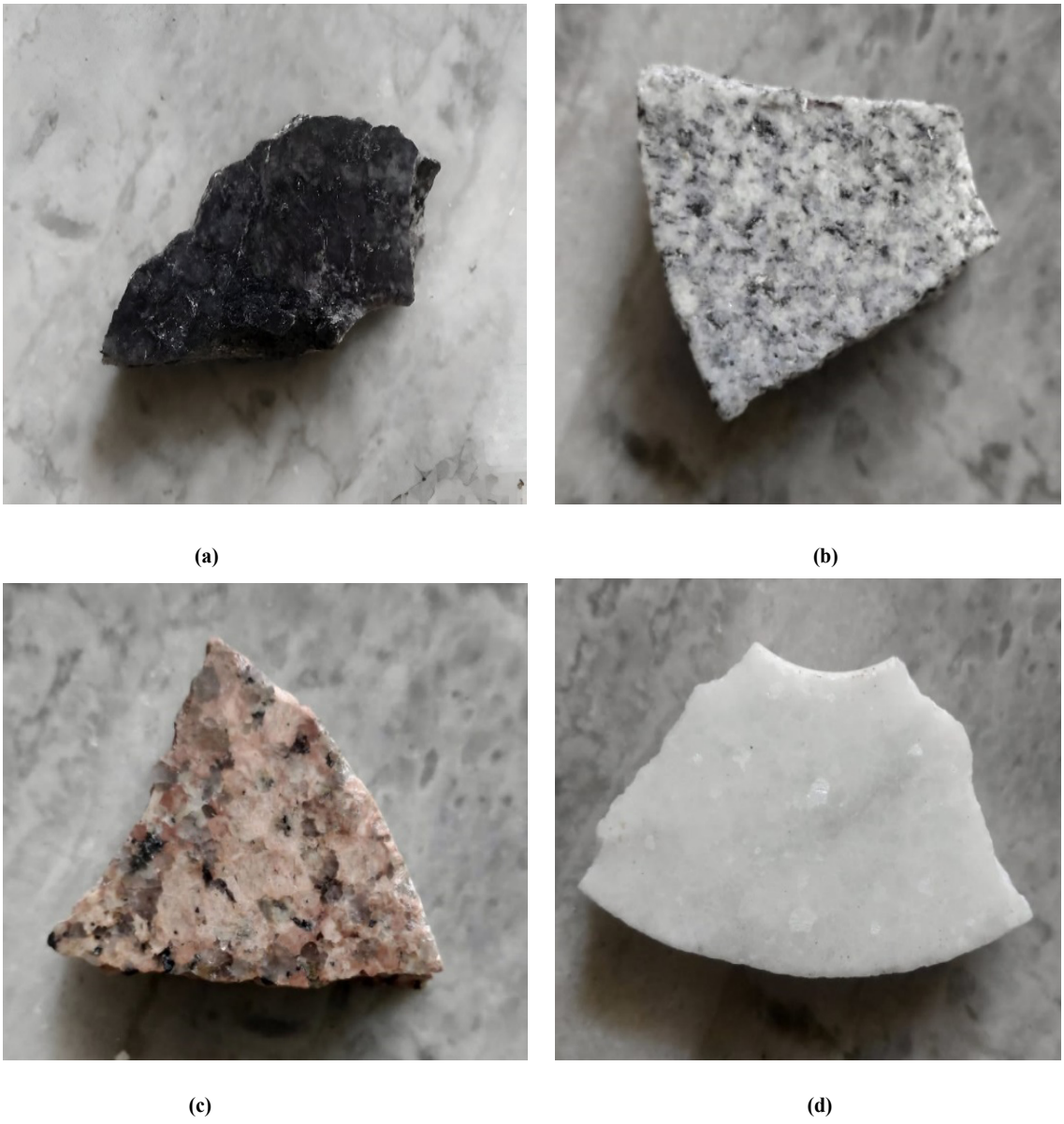


Figure 1. Various type of granite and marble used in the current study. **(a)** Dark Grey Granite from the Warangal District in Telangana. **(b)** Light Grey Granite from Jalore, Rajasthan. **(c)** Aswan Red Granite from Tamil Nadu (Krishnagiri). **(d)** White marble from Makrana, Rajasthan.

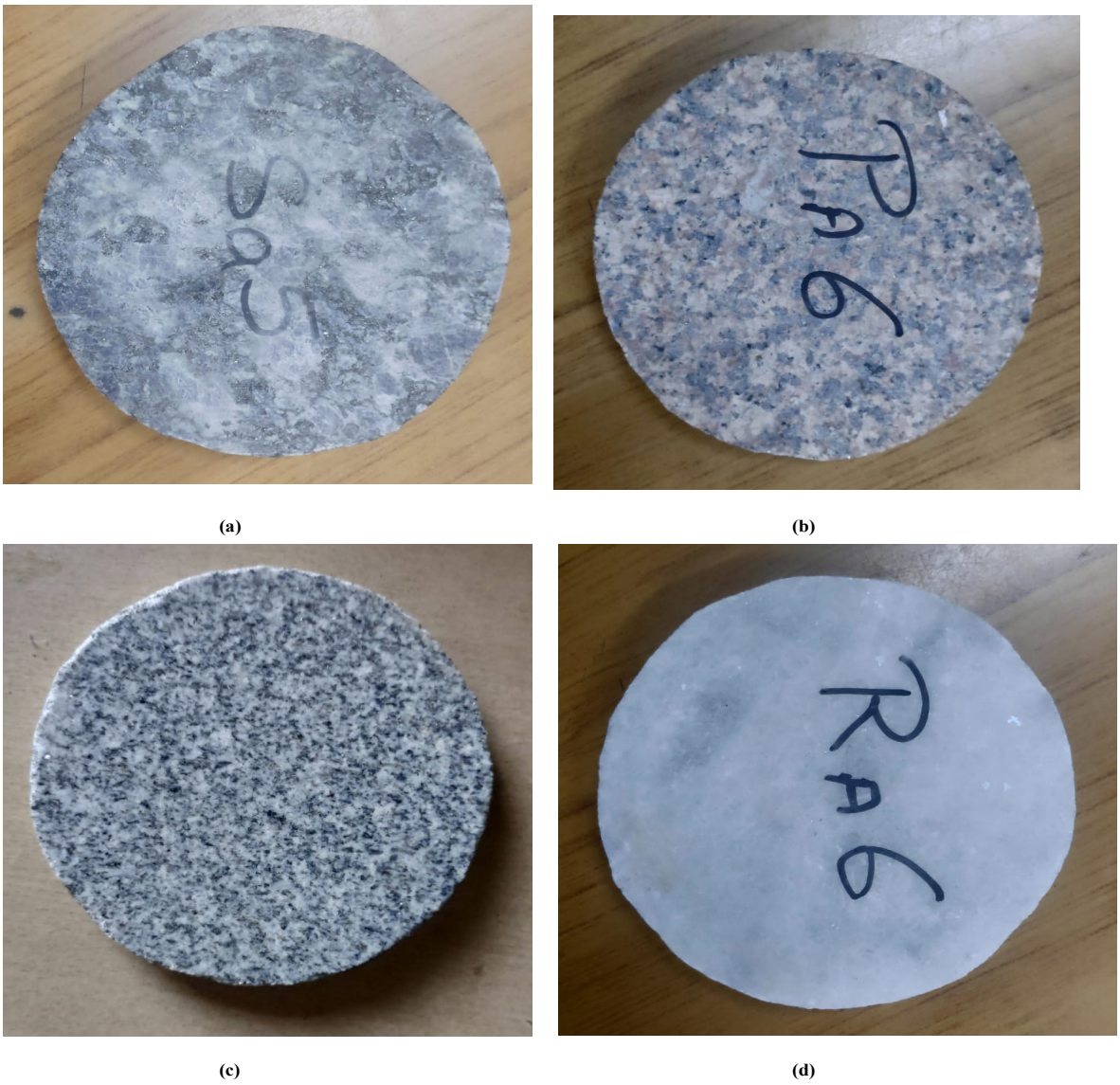


Figure 2. Brazilian disc specimens. **(a)** Brazilian disc specimen composed of dark grey granite. **(b)** Brazilian disc specimen composed of aswan red granite.**(c)** Brazilian disc specimen composed of light grey granite.**(d)** Brazilian disc specimen composed of marble.

uniform thickness and flatness, adhering to ISRM standards. To maintain consistency and avoid introducing micro-cracks, additional surface finishing was conducted using a fine-grit abrasive. Similar sample preparation techniques have been employed by other researchers for accurate assessment of mechanical properties in brittle materials.

3.0 Methods

The XRD analysis was performed using the X'Pert^3 MRD XL instrument, which utilizes Cu Kα radiation at a wavelength value of 1.54060 Å. The powdered samples of granite and marble were placed in the sample holder of the XRD instrument. The diffraction patterns that resulted from exposing the samples to Cu Kα radiation were then

recorded[42]. These data included key parameters such as the diffraction angle (2θ), the distance between lattice planes (d-spacing), the Full Width at Half Maximum (FWHM) of the peaks, and the Intensity (I) of the diffracted X-rays. By analysing the XRD patterns, the mineral phases present in the samples were identified. The diffraction peaks were matched with standard reference patterns from the XRD software's mineral database[43] , allowing for the identification of different minerals in the granite and marble samples. To highlight variations in their structural features, the average crystallite diameters and lattice strains for Aswan red granites, white marble, light grey granites, and dark grey granites were determined. The Scherrer equation[44] can be used to calculate the particle size.

$$\tau = \frac{K\lambda}{\beta cos\theta} \quad (1)$$

Where 'τ' is the average crystal size (nm), 'K' is Scherrer constant (0.9), 'λ' is X-ray wavelength (Å), is full width at half maximum (radians), and 'θ' is diffraction angle (°)

The mineral composition of the samples was plotted using XRD data and compared with SEM-EDS results. This comparison demonstrated the consistency of both approaches in determining the chemical makeup of the component oxides in granite and marble. The surface morphology of the granite and marble samples was investigated using a JSM-6390 scanning electron microscope (SEM)[45]. The experiment was conducted with specific parameters: a Working Distance (WD) of 14–17 mm, a high voltage (HV) of 10 kV, a signal type of Secondary Electron Imaging (SEI), and a magnification range of 190x to 10,000x. The elemental composition of the samples was determined using Energy-Dispersive X-Ray Spectroscopy (EDS).

Furthermore, to achieve a comprehensive mechanical characterization, the Brazilian indirect tensile test was conducted using a hydraulic loading frame supplied by engineering instruments. Disc-shaped specimens were positioned between hardened steel-platens, ensuring precise alignment along their diameters to promote uniform stress distribution during loading[46]. A uniaxial compressive load was applied at a constant displacement rate until tensile failure was induced along the vertical diametral plane. The peak load at failure was accurately recorded and employed to calculate the indirect tensile strength using the following equation:

$$\sigma_t = \frac{2P}{\pi Dt} \quad (2)$$

Where, σ_t is the tensile strength, P is the peak load at failure, D is the diameter of the specimen, and t is its thickness.

4.0 Results and Discussions

4.1 Mineral Phase

The minerals and crystals present in granite and marble have been established using X-Ray Diffraction (XRD). The experiment yielded parameters such as diffraction angle (2θ), Intensity (I), Full Width at Half Maximum (FWHM), and distance between fields (d). The mineral compositions of the marble and granite were determined by examining their diffraction peaks based on the relationship between diffraction angle (2θ) and Intensity (I). The XRD investigation of the granite and marble rock samples revealed the phase patterns depicted in Figure 3.

According to the X-ray Diffractometer's mineral database, the granite sample included the following mineral compositions at different diffraction angles: In addition to small amounts of calcium carbonate ($CaCO_3$), copper iron sulphide (Cu_5FeS_4), calcium fluoride (CaF_2), uranium oxide (UO_2), and praseodymium oxide ($PrO_{1.63}$), there are also silicon oxide (SiO_2), aluminium oxide (Al_2O_3), and sodium erbium fluoride ($NaErF_4$). White marble is mostly composed of calcium carbonate ($CaCO_3$) and calcium magnesium carbonate ($CaMg(CO_3)_3$), with trace amounts of silicon oxide (SiO_2).

4.2 Crystalline Size

The determination of crystalline sizes involves the expansion of the Full Width at Half Maximum (FWHM) of the X-ray diffraction peaks and the analysis of their positions. The standard FHWM value used at ° 2θ/ ° 2Thwas 0.008. β observed was analysed and structural β was calculated from the equation (2).

$$\beta_{structural} = \beta_{observed} - \beta_{standard} \quad (2)$$

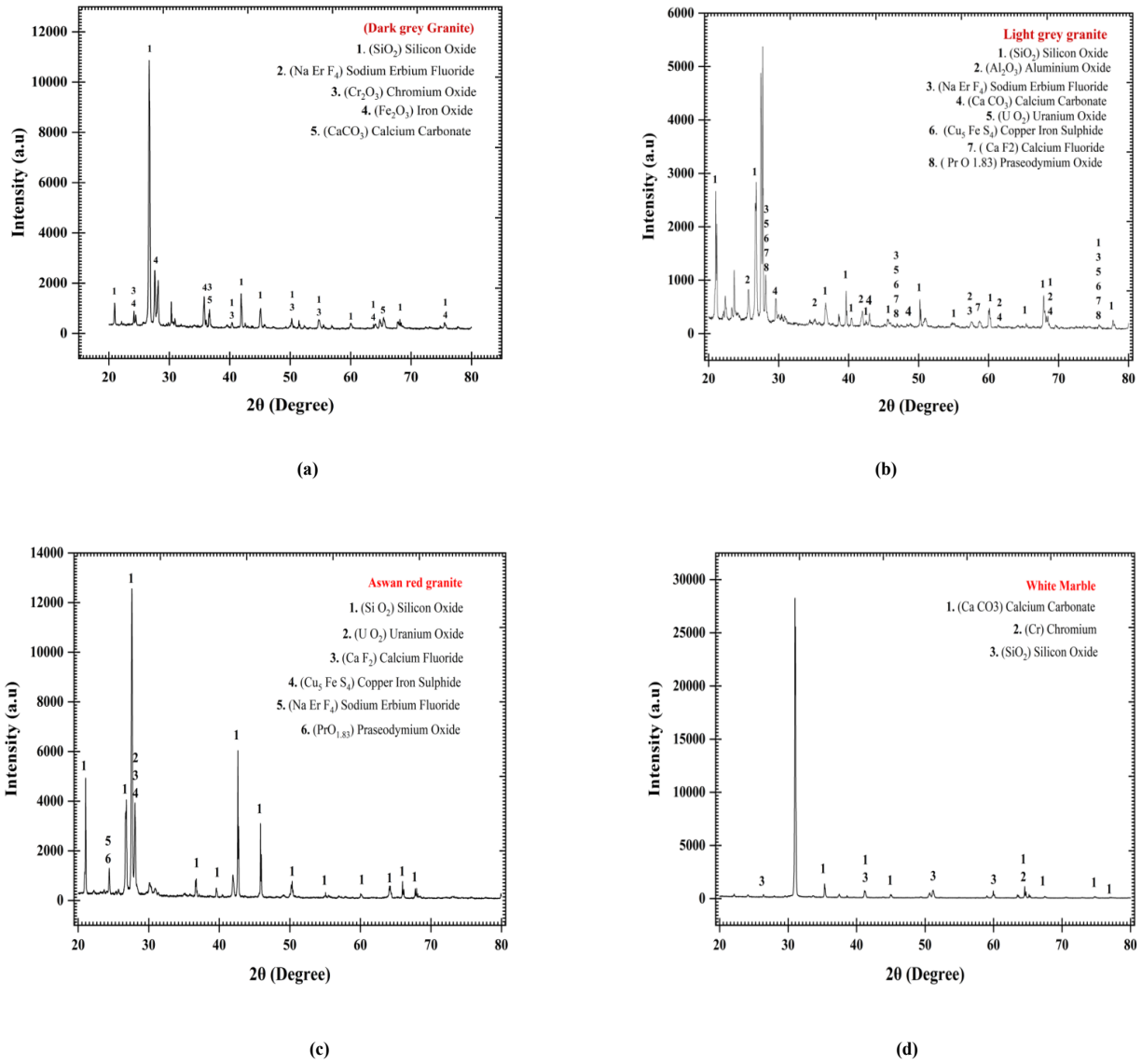


Figure 2. Phase pattern of various materials used. **(a)** Dark Grey Granite. **(b)** Dark Grey Granite. **(c)**Aswan Red Granite. **(d)** White Marble.

The crystalline sizes were determined using the Scherrer equation (1) and are presented in Tables 2, 3, 4 and 5 for dark grey granite, light grey granite, aswan red granite and white marble respectively. The average sizes of the crystals in Dark Grey Granite, Light Grey Granite, Aswan Red Granites, and White Marble were found to be 84.87 nm, 74.60 nm, 69.73 nm, and 71.60 nm, respectively. With increase in grain size overall strength of the specimen increases. The production of grain boundary cracks in response to loading and the quantity of formed smooth-joint contacts at grain interfaces are the primary mechanisms underlying the strength increase with increased grain size. The breadth of the diffraction peaks is inversely related to the size of the crystals; larger crystals lead to narrower peaks, while smaller crystals lead to wider peaks.

Table 2. Crystalline size of Dark grey granite specimen

S. No.	β obs. [°2Th]	β std. [°2Th]	Peak pos. [°2Th]	β struct. [°2Th]	Crystallite size [Å]
1	0.102	0.008	20.968	0.094	859
2	0.102	0.008	22.131	0.094	861
3	0.077	0.008	24.146	0.069	1177
4	0.077	0.008	24.459	0.069	1178
5	0.205	0.008	25.68	0.197	414
6	0.172	0.008	26.682	0.164	498
7	0.094	0.008	27.571	0.086	951
8	0.109	0.008	28.163	0.101	811
9	0.125	0.008	29.859	0.117	703
10	0.047	0.008	30.325	0.039	2110
11	0.047	0.008	30.91	0.039	2113
12	0.749	0.008	32.159	0.741	112
13	0.374	0.008	34.164	0.366	227
14	0.078	0.008	35.779	0.07	1193
15	0.062	0.008	36.079	0.054	1547
16	0.062	0.008	36.542	0.054	1549
17	0.078	0.008	36.635	0.07	1195
18	0.25	0.008	39.561	0.242	349
19	0.156	0.008	40.403	0.148	572
20	0.094	0.008	41.879	0.086	989
21	0.125	0.008	42.559	0.117	729
22	0.094	0.008	45.12	0.086	1000
23	0.25	0.008	45.759	0.242	356
24	0.499	0.008	47.238	0.491	177
25	0.125	0.008	50.272	0.117	750
26	0.094	0.008	51.434	0.086	1025
27	0.094	0.008	52.332	0.086	1029
28	0.156	0.008	54.696	0.148	604
29	0.25	0.008	55.489	0.242	371
30	0.094	0.008	56.873	0.086	1051

31	0.374	0.008	60.008	0.366	251
32	0.062	0.008	63.779	0.054	1733
33	0.218	0.008	64.149	0.21	446
34	0.187	0.008	64.805	0.179	526
35	0.187	0.008	65.427	0.179	527
36	0.094	0.008	67.73	0.086	1112
37	0.125	0.008	67.909	0.117	819
38	0.078	0.008	68.163	0.07	1370
39	0.187	0.008	72.425	0.179	550
40	0.125	0.008	74.821	0.117	855
41	0.156	0.008	75.507	0.148	679
42	0.374	0.008	77.814	0.366	279
				Average	848.7380952
					84.87nm

Table 3. Crystalline size of Light grey granite specimen

S. No.	B obs. [°2Th]	B std. [°2Th]	Peak pos. [°2Th]	B struct. [°2Th]	Crystallite size [Å]
1	0.074	0.008	21.006	0.066	1224
2	0.051	0.008	21.154	0.043	1879
3	0.093	0.008	22.11	0.085	952
4	0.142	0.008	22.385	0.134	604
5	0.094	0.008	23.31	0.086	943
6	0.087	0.008	23.653	0.079	1027
7	0.204	0.008	25.679	0.196	416
8	0.147	0.008	26.673	0.139	587
9	0.068	0.008	26.807	0.06	1361
10	0.082	0.008	27.476	0.074	1105
11	0.065	0.008	27.725	0.057	1436
12	0.161	0.008	28.13	0.153	535
13	0.046	0.008	28.391	0.038	2156
14	0.18	0.008	29.585	0.172	478
15	0.234	0.008	30.385	0.226	364

16	0.246	0.008	30.883	0.238	346
17	0.172	0.008	34.446	0.164	507
18	0.263	0.008	35.133	0.255	327
19	0.126	0.008	35.782	0.118	707
20	0.252	0.008	36.724	0.244	343
21	0.069	0.008	38.594	0.061	1380
22	0.074	0.008	39.648	0.066	1280
23	0.13	0.008	40.386	0.122	694
24	0.229	0.008	41.901	0.221	385
25	0.237	0.008	42.495	0.229	372
26	0.124	0.008	42.958	0.116	736
27	0.376	0.008	45.635	0.368	234
28	0.093	0.008	46.905	0.085	1019
29	0.732	0.008	48.718	0.724	120
30	0.067	0.008	50.188	0.059	1487
31	0.42	0.008	50.889	0.412	214
32	0.625	0.008	54.899	0.617	145
33	0.296	0.008	57.536	0.288	315
34	0.246	0.008	58.689	0.238	383
35	0.096	0.008	60.009	0.088	1042
36	0.084	0.008	60.114	0.076	1208
37	0.195	0.008	61.353	0.187	494
38	0.822	0.008	62.6	0.814	114
39	0.351	0.008	64.139	0.343	273
40	0.095	0.008	65.352	0.087	1085
41	0.158	0.008	67.855	0.15	638
42	0.257	0.008	68.342	0.249	386
43	0.12	0.008	69.572	0.112	864
44	0.17	0.008	75.769	0.162	621
45	0.138	0.008	77.77	0.13	785
				Average	746.0222222
					74.6 nm

Table 4. Crystalline size of Aswan red granites specimen

S. No.	β obs. [°2Th]	β std. [°2Th]	Peak pos. [°2Th]	β struct. [°2Th]	Crystallite size [Å]
1	0.064	0.008	21.054	0.056	1443
2	0.102	0.008	24.41	0.094	865
3	0.102	0.008	26.705	0.094	869
4	0.192	0.008	28.041	0.184	445
5	0.256	0.008	30.102	0.248	332
6	0.205	0.008	36.676	0.197	425
7	0.128	0.008	39.569	0.12	704
8	0.128	0.008	41.927	0.12	709
9	0.062	0.008	42.635	0.054	1579
10	0.062	0.008	45.845	0.054	1597
11	0.25	0.008	50.255	0.242	363
12	0.312	0.008	60.095	0.304	302
13	0.25	0.008	64.149	0.242	387
14	0.312	0.008	65.943	0.304	311
15	0.749	0.008	67.984	0.741	129
				Average	697.3333333
					69.73 nm

Table 5. Crystalline size of White marble

S. No.	β obs. [°2Th]	β std. [°2Th]	Peak pos. [°2Th]	β struct. [°2Th]	Crystallite size [Å]
1	0.083	0.008	26.39	0.075	1088
2	0.078	0.008	27.943	0.07	1169
3	0.201	0.008	29.545	0.193	426
4	0.245	0.008	30.015	0.237	347
5	0.093	0.008	30.99	0.085	970
6	0.099	0.008	31.088	0.091	906

7	0.419	0.008	33.617	0.411	202
8	0.093	0.008	35.332	0.085	981
9	0.139	0.008	37.438	0.131	640
10	0.047	0.008	38.606	0.039	2158
11	0.14	0.008	39.577	0.132	640
12	0.122	0.008	41.154	0.114	744
13	0.122	0.008	41.286	0.114	745
14	0.379	0.008	48.699	0.371	235
15	0.21	0.008	49.348	0.202	433
16	0.218	0.008	50.623	0.21	418
17	0.218	0.008	51.14	0.21	419
18	0.244	0.008	52.262	0.236	375
19	0.139	0.008	54.94	0.131	683
20	0.114	0.008	59.026	0.106	861
21	0.116	0.008	59.955	0.108	849
22	0.109	0.008	63.49	0.101	925
23	0.076	0.008	64.549	0.068	1382
24	0.078	0.008	65.182	0.07	1347
25	0.212	0.008	65.285	0.204	462
26	0.307	0.008	66.144	0.299	317
27	0.17	0.008	67.479	0.162	590
28	0.215	0.008	70.567	0.207	470
29	0.195	0.008	77.929	0.187	546
30	0.224	0.008	74.768	0.216	463
31	0.259	0.008	77.08	0.251	405
				Average	716
					71.6 nm

4.3 Crystallite Lattice Strain

The crystallite lattice strain, which was calculated using the Scherrer equation, is tabulated in Table 6, 7, 8, and 9 for dark grey granite, light grey granite, aswan red granite and white marble respectively. The average crystallite lattice strains counted from dark grey, light grey, Aswan red granites, and white marble were 0.188%, 0.222%, 0.221%, and 0.173%, respectively. Crystallite lattice strain was higher in all granite specimens, i.e., dark grey, light

Table 6. Crystallite lattice strain of dark grey granite specimen

S. No.	β obs. [°2Th]	β std. [°2Th]	Peak pos. [°2Th]	β struct. [°2Th]	Lattice strain [%]
1	0.102	0.008	20.968	0.102	0.24
2	0.102	0.008	22.131	0.102	0.227
3	0.077	0.008	24.146	0.077	0.156
4	0.077	0.008	24.459	0.077	0.154
5	0.205	0.008	25.68	0.205	0.392
6	0.172	0.008	26.682	0.172	0.316
7	0.094	0.008	27.571	0.094	0.167
8	0.109	0.008	28.163	0.109	0.189
9	0.125	0.008	29.859	0.125	0.204
10	0.047	0.008	30.325	0.046	0.075
11	0.047	0.008	30.91	0.046	0.073
12	0.749	0.008	32.159	0.749	1.134
13	0.374	0.008	34.164	0.374	0.531
14	0.078	0.008	35.779	0.078	0.105
15	0.062	0.008	36.079	0.061	0.082
16	0.062	0.008	36.542	0.061	0.081
17	0.078	0.008	36.635	0.078	0.102
18	0.25	0.008	39.561	0.25	0.303
19	0.156	0.008	40.403	0.156	0.185
20	0.094	0.008	41.879	0.094	0.107
21	0.125	0.008	42.559	0.125	0.14
22	0.094	0.008	45.12	0.094	0.098
23	0.25	0.008	45.759	0.25	0.258
24	0.499	0.008	47.238	0.499	0.498
25	0.125	0.008	50.272	0.125	0.116
26	0.094	0.008	51.434	0.094	0.085
27	0.094	0.008	52.332	0.094	0.083

28	0.156	0.008	54.696	0.156	0.131
29	0.25	0.008	55.489	0.25	0.207
30	0.094	0.008	56.873	0.094	0.075
31	0.374	0.008	60.008	0.374	0.283
32	0.062	0.008	63.779	0.061	0.043
33	0.218	0.008	64.149	0.218	0.152
34	0.187	0.008	64.805	0.187	0.128
35	0.187	0.008	65.427	0.187	0.127
36	0.094	0.008	67.73	0.094	0.061
37	0.125	0.008	67.909	0.125	0.081
38	0.078	0.008	68.163	0.078	0.05
39	0.187	0.008	72.425	0.187	0.111
40	0.125	0.008	74.821	0.125	0.071
41	0.156	0.008	75.507	0.156	0.088
42	0.374	0.008	77.814	0.374	0.202
				Average	0.188

Table 7. Crystallite lattice strain of light grey granite specimen

S. No.	β obs. [°2Th]	β std. [°2Th]	Peak pos. [°2Th]	β struct. [°2Th]	Lattice strain [%]
1	0.074	0.008	21.006	0.074	0.173
2	0.051	0.008	21.154	0.05	0.118
3	0.093	0.008	22.11	0.093	0.207
4	0.142	0.008	22.385	0.142	0.313
5	0.094	0.008	23.31	0.094	0.198
6	0.087	0.008	23.653	0.087	0.181
7	0.204	0.008	25.679	0.204	0.39
8	0.147	0.008	26.673	0.147	0.27
9	0.068	0.008	26.807	0.068	0.124
10	0.082	0.008	27.476	0.082	0.146
11	0.065	0.008	27.725	0.065	0.114
12	0.161	0.008	28.13	0.161	0.28
13	0.046	0.008	28.391	0.045	0.078
14	0.18	0.008	29.585	0.18	0.297

15	0.234	0.008	30.385	0.234	0.376
16	0.246	0.008	30.883	0.246	0.388
17	0.172	0.008	34.446	0.172	0.242
18	0.263	0.008	35.133	0.263	0.362
19	0.126	0.008	35.782	0.126	0.17
20	0.252	0.008	36.724	0.252	0.331
21	0.069	0.008	38.594	0.069	0.085
22	0.074	0.008	39.648	0.074	0.089
23	0.13	0.008	40.386	0.13	0.154
24	0.229	0.008	41.901	0.229	0.261
25	0.237	0.008	42.495	0.237	0.266
26	0.124	0.008	42.958	0.124	0.137
27	0.376	0.008	45.635	0.376	0.39
28	0.093	0.008	46.905	0.093	0.093
29	0.732	0.008	48.718	0.732	0.705
30	0.067	0.008	50.188	0.067	0.062
31	0.42	0.008	50.889	0.42	0.385
32	0.625	0.008	54.899	0.625	0.525
33	0.296	0.008	57.536	0.296	0.235
34	0.246	0.008	58.689	0.246	0.191
35	0.096	0.008	60.009	0.096	0.072
36	0.084	0.008	60.114	0.084	0.063
37	0.195	0.008	61.353	0.195	0.143
38	0.822	0.008	62.6	0.822	0.59
39	0.351	0.008	64.139	0.351	0.244
40	0.095	0.008	65.352	0.095	0.064
41	0.158	0.008	67.855	0.158	0.102
42	0.257	0.008	68.342	0.257	0.165
43	0.12	0.008	69.572	0.12	0.075
44	0.17	0.008	75.769	0.17	0.095
45	0.138	0.008	77.77	0.138	0.075
				Average	0.223

Table 8. Crystallite lattice strain of aswan red granites specimen

S. No.	β obs. [°2Th]	β std. [°2Th]	Peak pos. [°2Th]	β struct. [°2Th]	Lattice strain [%]
1	0.064	0.008	21.054	0.063	0.149
2	0.102	0.008	24.41	0.102	0.205
3	0.102	0.008	26.705	0.102	0.187
4	0.192	0.008	28.041	0.192	0.335
5	0.256	0.008	30.102	0.256	0.415
6	0.205	0.008	36.676	0.205	0.27
7	0.128	0.008	39.569	0.128	0.155
8	0.128	0.008	41.927	0.128	0.145
9	0.062	0.008	42.635	0.061	0.069
10	0.062	0.008	45.845	0.061	0.063
11	0.25	0.008	50.255	0.25	0.232
12	0.312	0.008	60.095	0.312	0.235
13	0.25	0.008	64.149	0.25	0.174
14	0.312	0.008	65.943	0.312	0.21
15	0.749	0.008	67.984	0.749	0.485
				Average	0.222

Table 9. Crystallite lattice strain of white marble specimen

S. No.	β obs. [°2Th]	β std. [°2Th]	Peak pos. [°2Th]	β struct. [°2Th]	Lattice strain [%]
1	0.083	0.008	26.39	0.083	0.154
2	0.078	0.008	27.943	0.078	0.136
3	0.201	0.008	29.545	0.201	0.332
4	0.245	0.008	30.015	0.245	0.399
5	0.093	0.008	30.99	0.093	0.146
6	0.099	0.008	31.088	0.099	0.155
7	0.419	0.008	33.617	0.419	0.605

8	0.093	0.008	35.332	0.093	0.127
9	0.139	0.008	37.438	0.139	0.179
10	0.047	0.008	38.606	0.046	0.058
11	0.14	0.008	39.577	0.14	0.17
12	0.122	0.008	41.154	0.122	0.141
13	0.122	0.008	41.286	0.122	0.141
14	0.379	0.008	48.699	0.379	0.365
15	0.21	0.008	49.348	0.21	0.199
16	0.218	0.008	50.623	0.218	0.201
17	0.218	0.008	51.14	0.218	0.199
18	0.244	0.008	52.262	0.244	0.217
19	0.139	0.008	54.94	0.139	0.116
20	0.114	0.008	59.026	0.114	0.088
21	0.116	0.008	59.955	0.116	0.088
22	0.109	0.008	63.49	0.109	0.077
23	0.076	0.008	64.549	0.076	0.052
24	0.078	0.008	65.182	0.078	0.053
25	0.212	0.008	65.285	0.212	0.144
26	0.307	0.008	66.144	0.307	0.206
27	0.17	0.008	67.479	0.17	0.111
28	0.215	0.008	70.567	0.215	0.132
29	0.195	0.008	77.929	0.195	0.105
30	0.224	0.008	74.768	0.224	0.128
31	0.259	0.008	77.08	0.259	0.142
				Average	0.173

grey, and Aswan red granites, which leads to increased hardness, brittleness, and higher chances of microcrack formation compared to white marble. The white marble with the least crystallite lattice strain minimises surface defects, enhancing the aesthetic quality and smooth finish.

4.4 Surface Morphology studies

The presence of elements on the surfaces of marble and granite were confirmed using FESEM-EDS analysis. Figures 4 illustrate the physical characteristics of the surface microcracks found on the various marble and granite specimens. The surface morphology was visualized by catching and analysing secondary electrons generated by the test materials. The photos depict the surface morphology of granite and marble stone samples at magnifications of 190x and 5000x, respectively. When observed at greater magnifications, the crystal formations exhibit a more distinct and well-defined appearance. The photos depict particles with odd shapes and angles, which are likely a result of impurities that results in the generation of new phases. The elemental content of the investigated samples was determined by combining the SEM analysis with Energy Dispersive X-Ray Spectroscopy (EDS).

Figures 5 display the outcomes of EDS characterisation for granite and marble stones obtained from different sites. The EDS spectrum analysis reveals the existence of Carbon (C), Sodium (Na), Oxygen (O), Silicon (Si), Aluminium (Al), Potassium (K), Iron (Fe), Calcium (Ca), and Magnesium (Mg) in the granite and marble samples. Table 10 displays the elemental makeup, providing the weight in terms of percentage and atomic percentage for each element. From the results, the element content of

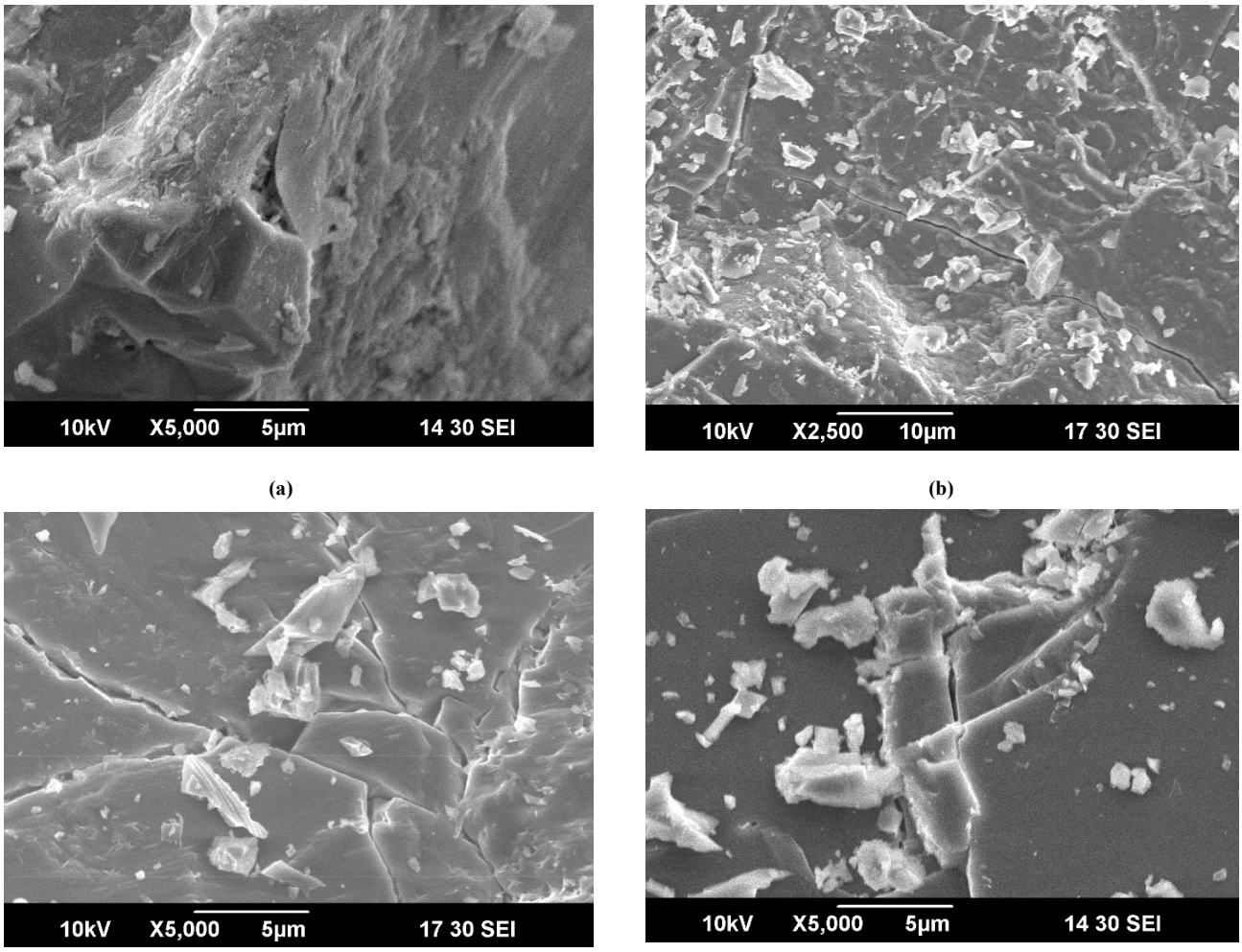


Figure 4. FESEM image of various test specimens with microcracks. **(a)** Dark grey granite. **(b)** Light grey granite. **(c)** Aswan Red Granite. **(d)** White marble.

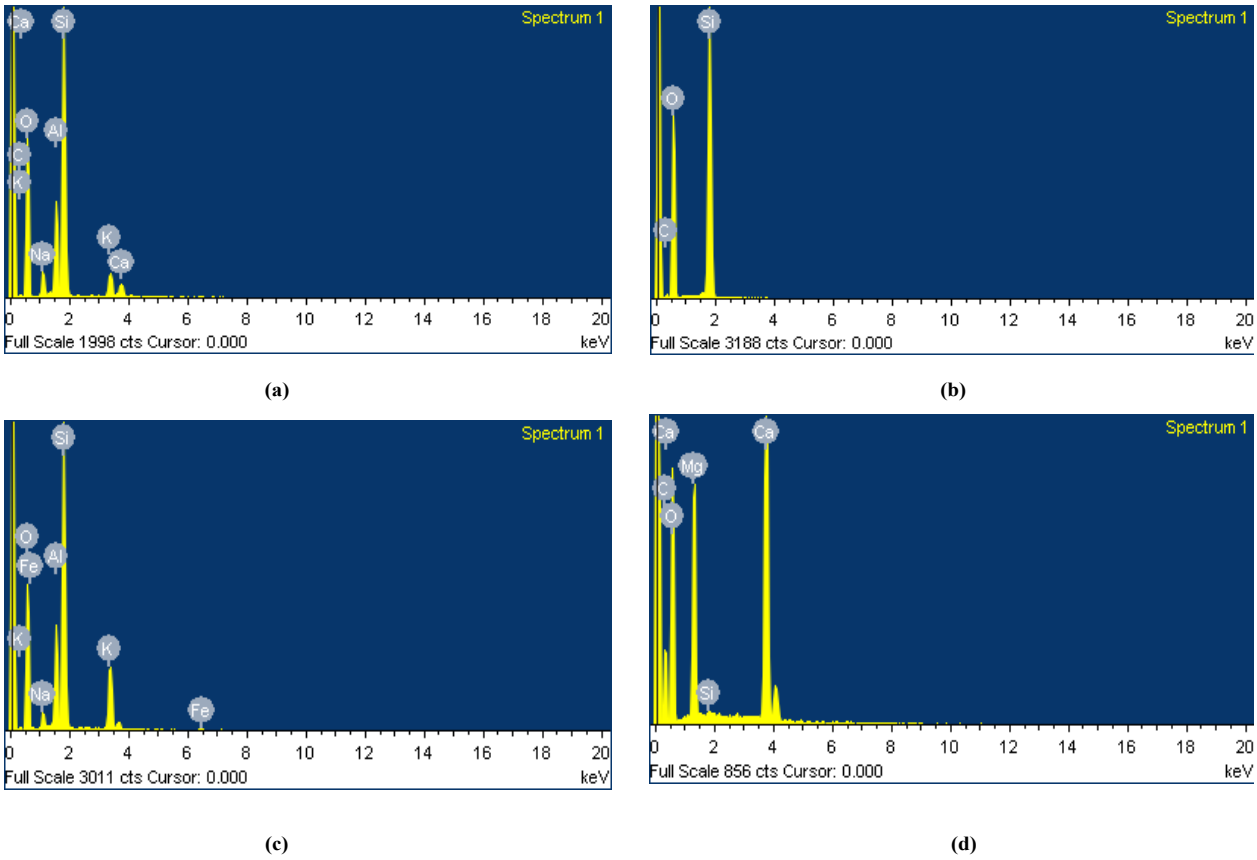


Figure 5. EDS Spectrum of various specimens used in the study. **(a)** Dark grey granite. **(b)** Light grey granite. **(c)** Aswan red granite. **(d)** White marble.

Table 10. Elemental composition of dark grey granite, light grey granite, aswan red granite and white marble (with weight % and atomic %)

Element	Dark Grey Granite	Light Grey Granite	Aswan Red Granite	White Marble	Dark Grey Granite	Light Grey Granite	Aswan Red Granite	White Marble
	(weight %)	(weight %)	(weight %)	(weight %)	(Atomic %)	(Atomic %)	(Atomic %)	(Atomic %)
C	3.13	6.08	--	16.54	5.03	9.05	--	24.07
O	55.59	64.90	54.29	55.64	66.93	72.49	68.47	60.83
Na	3.12	--	2.16	--	2.61	--	1.89	--
Al	7.81	--	8.23	--	5.57	--	6.16	--
Si	25.45	29.02	26.41	0.14	17.47	18.46	18.97	0.09
K	3.05	--	8.29	--	1.50	--	4.28	--
Ca	1.85	--	--	17.33	0.89	--	--	7.56
Fe	--	--	0.62	--	--	--	0.23	--
Mg	--	--	--	10.35	--	--	--	7.45
Total	**100**	**100**	**100**	**100**	**100**	**100**	**100**	**100**

oxygen in granite stones and white marble, was found to be in the range of 54.29% to 64.90%, making it the highest among all the other elements. Furthermore, the granite specimens exhibit a higher silicon content in comparison to the white marble.

4.5 Tensile Strength

Figure 6 illustrates the application of the Brazilian disc method for quantifying the tensile strength of rocks, specifically highlighting fracture mode I propagation.

Table 11. Tensile Strength and Geometric Properties of Aswan Red Granite, Light Grey Granite, White Marble, and Dark Grey Granite Specimens

Specimen Type	Specimen No	Weight (gm)	Diameter (cm)	Thickness (cm)	Displacement (mm)	Failure load (kN)	σ_t (MPa)
Aswan red granite	Pa1	335.85	12.19	1.73	0.41	45.1	1.36
	Pa2	334.80	12.21	1.67	0.39	44.8	1.40
	Pa3	335.75	12.18	1.71	0.37	44.7	1.37
	Pa4	338.40	12.17	1.69	0.40	44.9	1.39
	Pa5	331.40	12.15	1.68	0.41	43.9	1.37
	Pa6	333.50	12.04	1.75	0.39	44.6	1.35
Average							**1.37**
Light grey granite	Qa1	357.65	12.05	1.73	0.35	46.5	1.42
	Qa2	355.05	11.91	1.79	0.31	45.2	1.35
	Qa3	351.75	12.04	1.66	0.32	45.6	1.45
	Qa4	352.65	12.21	1.59	0.34	46.1	1.51
	Qa5	352.80	11.96	1.55	0.33	45.5	1.56
	Qa6	350.70	12.03	1.71	0.34	44.7	1.38
Average							**1.45**
White Marble	Ra1	354.98	12.09	1.45	0.46	24.9	0.90
	Ra2	353.67	12.05	1.41	0.47	24.7	0.93
	Ra3	357.60	11.96	1.42	0.44	23.9	0.90
	Ra4	356.70	12.12	1.43	0.46	24.8	0.91
	Ra5	353.95	12.23	1.42	0.47	25	0.92
	Ra6	355.65	12.19	1.48	0.45	23.2	0.82
Average							**0.89**
Dark grey granite	Sa1	311.47	12.21	1.51	0.43	41.9	1.45
	Sa2	315.46	12.24	1.53	0.38	41.6	1.41
	Sa3	310.80	12.06	1.44	0.41	41.2	1.51
	Sa4	317.46	12.63	1.54	0.42	40.6	1.33
	Sa5	316.40	12.26	1.51	0.39	42.1	1.45
	Sa6	314.75	12.54	1.53	0.40	41.5	1.38
Average							**1.42**



Figure 6. Brazilian disc method for determination of tensile strength of rocks.

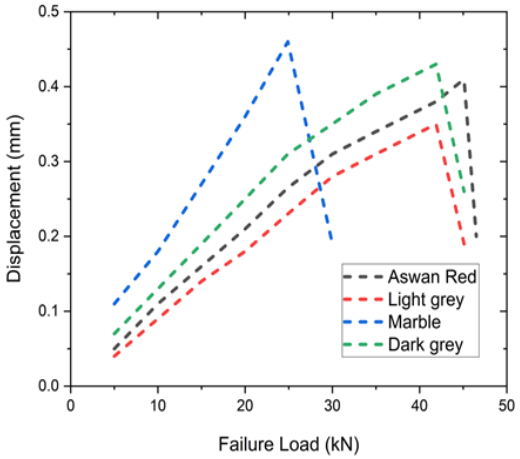


Figure 7. Load-displacement curve generated from the brazilian disc test with various granite and marble specimens.

The experimentally determined tensile strength values for Aswan red granite, light grey granite, white marble, and dark grey granite are documented in Table 11. The average tensile strength measurements obtained for these lithologies are 1.37 MPa, 1.45 MPa, 0.89 MPa, and 1.42 MPa, respectively. Notably, light grey granite exhibited the highest tensile strength among the tested specimens, underscoring its superior resistance to tensile failure compared to the other rock types. In contrast, white marble displayed the lowest tensile strength, attributable to its lower density and intrinsic structural composition, rendering it more susceptible to tensile fracture initiation and propagation[47]. The proximate tensile strength values observed for dark grey granite and Aswan red granite suggest analogous tensile failure mechanisms, likely due to their comparable mineralogical compositions and microstructural features. Figure 7 presents the load-displacement curves derived from the Brazilian disc tests conducted on the various granite and marble specimens, providing insights into their mechanical responses under tensile loading conditions.

5.0 Conclusions

The objective of the current study was to analyse the mineral composition of various types of granite stones, including dark grey, light grey, and Aswan red variations, as well as white marble and to these findings with their tensile strength properties. The current investigation can lead to the following conclusions.

- XRD analysis identified SiO_2 and Al_2O_3 as the primary mineral constituents, with minor phases including $NaErF_4$, $CaCO_3$, Cu_5FeS_4, CaF_2, UO_2, and $PrO_{1.83}$. EDS-XRD confirmed SiO_2 as the predominant phase, significantly enhancing granite's mechanical hardness and tensile strength.
- White marble is primarily composed of calcium carbonate ($CaCO_3$) and calcium magnesium carbonate ($CaMg(CO_3)_2$), with traces of silicon dioxide (SiO_2). High calcium (17.33 %) and magnesium (10.35 %) levels suggest a composition rich in softer calcite and dolomite, which are less resistant to tensile stress compared to quartz in granite.
- Tensile strength results from the Brazilian disc method demonstrate the impact of mineral composition on mechanical properties. Light grey granite shows the highest tensile strength (1.45 MPa) due to its high silica content and crystalline structure, while white marble exhibits the lowest (0.89 MPa) because of its high calcite and dolomite content, which offer less resistance to fracture under tensile stress.
- Carbon (C), Sodium (Na), Oxygen (O), Silicon (Si), Aluminium (Al), Potassium (K), Iron (Fe), Calcium (Ca), and Magnesium (Mg) were

identified in the sample using EDS analysis. The presence of trace elements like mentioned above in granite facilitates the formation of feldspar minerals, which possess strong adhesive properties that improve the rock's structural integrity, thereby increasing its tensile strength. The lower concentration of these elements in white marble corresponds with its lowered tensile strength.

- Oxygen content ranged from 54.29 % to 64.90 % in both granite and marble, reflecting the abundance of oxide minerals in these rocks. Granite's higher silicon content (25.45 % - 26.41 %) compared to white marble underscores the role of silicon dioxide in enhancing tensile strength due to its strong covalent bonding and rigid crystalline structure.
- Dark grey granite and Aswan red granite exhibited tensile strengths of 1.42 MPa and 1.37 MPa, respectively. These similar values validate the mineralogical analyses, suggesting comparable silicon dioxide content and microstructural characteristics that influence their mechanical behaviour under tensile stress.
- The load-displacement curves produced from the Brazilian disc tests (Figure 7) show the specimens' mechanical reactions to tensile loading conditions. The curves show that granites, with higher silicon dioxide content and favorable crystalline structures, exhibit greater resistance to deformation and failure compared to marble.
- The study effectively validates the correlation between mineral composition and tensile strength. The higher tensile strength of granites is consistent with their mineralogical makeup, rich in silicon dioxide and feldspar minerals, which contribute to their hardness and structural integrity. In contrast, the lower tensile strength of white marble aligns with its composition of softer carbonate minerals, confirming that mineralogical properties are critical determinants of tensile strength in rocks.

6.0 Acknowledgements

The authors would like to express their sincere gratitude to the Thapar Institute of Engineering and Technology, Patiala, Punjab, India and NIT Kurukshetra, Haryana, India for their valuable support and use of advanced instrumentation for the successful completion of this research.

7.0 References

1. Ismael IS, Hassan MS. Characterization of some Egyptian serpentinites used as ornamental stones. Chin J Geochem. 2008; 27(2):140-9. https://doi.org/10.1007/s11631-008-0140-0
2. Punturo R, Ricchiuti C, Rizzo M, Marrocchino E. Mineralogical and microstructural features of Namibia marbles: insights about tremolite related to natural asbestos occurrences. Fibers. 2019; 7(4):31. https://doi.org/10.3390/fib7040031
3. Bağcı M. Mineralogical, petrographic, and geochemical characterization of colored İscehisar marbles (Afyonkarahisar, W-Turkey). Turk J Earth Sci. 2020; 29(6):946-75. https://doi.org/10.3906/yer-2001-20
4. Lindawati L, Mursal M, Afdhal A. Determination of mineral contents in Meukek marble using XRD and SEM-EDS analysis. IOP Conf Ser Mater Sci Eng. 2019; 506:012023. https://doi.org/10.1088/1757-899X/506/1/012023
5. Qiu B, Wang F, Luo H, Holé C, Wang T, Zhu J, *et al.* Characterization and thermal behavior of granite waste during heating. Ceram Int. 2023; 49(11):17052-9. https://doi.org/10.1016/j.ceramint.2023.02.066
6. Pabiś-Mazgaj E, Gawenda T, Pichniarczyk P, Stempkowska A. Mineral composition and structural characterization of the clinoptilolite powders obtained from zeolite-rich tuffs. Minerals. 2021; 11(10):1030. https://doi.org/10.3390/min11101030
7. Song F, Dong YH, Xu ZF, Zhou PP, Wang LH, Tong SQ, *et al.* Granite microcracks: structure and connectivity at different depths. J Asian Earth Sci. 2016; 124:156-68. https://doi.org/10.1016/j.jseaes.2016.04.023
8. Jagadesh P, Oyebisi S, Muthu AH, Sarulatha A, Supikshaa K, Vhishva Laxmy VP. Microscopic analyses and performance characteristics of granite powder blended cement. Constr Build Mater. 2024; 426:136006. https://doi.org/10.1016/j.conbuildmat.2024.136006
9. Shang X, Zhang Z, Xu X, Liu T, Xing Y. Mineral composition, pore structure, and mechanical characteristics of pyroxene granite exposed to heat treatments. Minerals. 2019; 9(9):553. https://doi.org/10.3390/min9090553
10. Singh K, Lohchab RK, Kumar V, Kumar A. Degradation of ammonaical nitrogen (NH3-N) in leachate by zinc

oxide loaded activated carbon: process parameters modelling and optimization through RSM design. Bioresour Technol Rep. 2023; 24:101602. https://doi.org/10.1016/j.biteb.2023.101602
11. Singh K, Lohchab RK, Kumari M. Impregnation of zinc oxide nanoparticles on activated carbon synthesised from corncob for appraisal of leachate chemical oxygen demand removal potential. Int J Environ Anal Chem. 2022; 1-24. https://doi.org/10.1080/03067319.2022.2100256
12. Costa FP, Fernandes JV, Melo LRL, Rodrigues AM, Menezes RR, Neves GA. The potential for natural stones from northeastern Brazil to be used in civil construction. Minerals. 2021; 11(5):440. https://doi.org/10.3390/min11050440
13. Srijan S, Gupta AK. Horizontally layered and vertically encased geosynthetic reinforced stone column: an experimental analysis. Appl Sci. 2023; 13(15):8660. https://doi.org/10.3390/app13158660
14. Cowie S, Walton G. The effect of mineralogical parameters on the mechanical properties of granitic rocks. Eng Geol. 2018; 240:204-25. https://doi.org/10.1016/j.enggeo.2018.04.021
15. Javid A, Pandey BK, Srijan. Performance evaluation of clayey soil considering impact of lime during electrokinetic consolidation. Arab J Sci Eng. 2023; 49:4527-37. https://doi.org/10.1007/s13369-023-08148-2
16. Zhu ZN, Tian H, Jiang GS, Cheng W. Effects of high temperature on the mechanical properties of Chinese marble. Rock Mech Rock Eng. 2018; 51(6):1937-42. https://doi.org/10.1007/s00603-018-1426-0
17. Wang X, Liou JG. Ultra-high-pressure metamorphism of carbonate rocks in the Dabie Mountains, central China. J Metamorph Geol. 1993; 11(4):575-88. https://doi.org/10.1111/j.1525-1314.1993.tb00173.x
18. Chakhmouradian AR, Reguir EP, Zaitsev AN. Calcite and dolomite in intrusive carbonatites. I. Textural variations. Mineral Petrol. 2016; 110(2-3):333-60. https://doi.org/10.1007/s00710-015-0390-6
19. Srijan S, Kumar P, Aggarwal V, Walia BS. The unique modified seesaw test (MST) instrument for the direct assessment of rock's tensile strength utilizing ring-shaped specimens. Sādhanā. 2025; 50(3):1-13. https://doi.org/10.1007/s12046-025-02803-0
20. Nandy M. Neutron activation analysis: application in geology and medicine. In: Advanced technologies and applications of neutron activation analysis. IntechOpen; 2019; 1-12. https://doi.org/10.5772/intechopen.76726
21. Gauri KL, Hagerty DJ, Ullrich CR. Comparative physical properties of weathered impregnated and unimpregnated marble. Eng Geol. 1972; 6(4):235-50. https://doi.org/10.1016/0013-7952(72)90009-9
22. Johnson C, Pownceby MI, Wilson NC. The application of automated electron beam mapping techniques to the characterisation of low grade, fine-grained mineralisation; potential problems and recommendations. Miner Eng. 2015; 79:68-83. https://doi.org/10.1016/j.mineng.2015.05.005
23. Abdelgadir M, Yagob AA, Elzain AEA, Idris MA, Yagoob SI. Application of X-ray diffraction method for characterization of crystalline basalt samples. J Geol Soc India. 2024; 100(4):572-80. https://doi.org/10.17491/jgsi/2024/173874
24. Khan MM, Mahajani SM, Jadhav GN. Transformation of bentonite used in green sand molds during metal casting process and its relevance in sand reclamation. Appl Clay Sci. 2021; 206:106072. https://doi.org/10.1016/j.clay.2021.106072
25. Srijan, Gupta AK. A Review article on Construction, Parametric Study and Settlement Behavior of Stone Column. IOP Conference Series: Earth and Environmental Science. 796(1): 012021. https://doi.org/10.1088/1755-1315/796/1/012021
26. Freeman JJ, Wang A, Kuebler KE, Jolliff BL, Haskin LA. Characterization of natural feldspars by Raman spectroscopy for future planetary exploration. Can Mineral. 2008; 46(6):1477-500. https://doi.org/10.3749/canmin.46.6.1477
27. Jozanikohan G, Abarghooei MN. The Fourier transform infrared spectroscopy (FTIR) analysis for the clay mineralogy studies in a clastic reservoir. J Pet Explor Prod Technol. 2022; 12(8):2093-106. https://doi.org/10.1007/s13202-021-01449-y
28. Federico L, Crispini L, Capponi G, Bradshaw JD. The Cambrian Ross Orogeny in northern Victoria Land (Antarctica) and New Zealand: a synthesis. Gondwana Res. 2009; 15(2):188-96. https://doi.org/10.1016/j.gr.2008.10.004
29. Bain JA, Morgan DJ. The role of thermal analysis in the evaluation of impure clay deposits as mineral raw materials. Clay Miner. 1969; 8(2):171-92. https://doi.org/10.1180/claymin.1969.008.2.06
30. Angulo SC, Ulsen C, John VM, Kahn H, Cincotto MA. Chemical-mineralogical characterization of C&D waste recycled aggregates from São Paulo, Brazil. Waste Manag. 2009; 29(2):721-30. https://doi.org/10.1016/j.wasman.2008.07.009

31. Lowson RT, Comarmond MCJ, Rajaratnam G, Brown PL. The kinetics of the dissolution of chlorite as a function of pH and at 25°C. Geochim Cosmochim Acta. 2005; 69(7):1687-99. https://doi.org/10.1016/j.gca.2004.09.028
32. González-Blanco C, Rodríguez LJ, Velázquez MM. Effect of the Solvent on the Water Properties of Water/Oil Microemulsions. J Colloid Interface Sci. 1999; 211(2):380–6.
33. Malek MA, Nakazawa T, Kang HW, Tsuji K, Ro CU. Multi-Modal Compositional Analysis of Layered Paint Chips of Automobiles by the Combined Application of ATR-FTIR Imaging, Raman Microspectrometry, and SEM/EDX. Molecules. 2019; 24(7):1381.
34. Kularatne K, Audétat A. Rutile solubility in hydrous rhyolite melts at 750–900°C and 2kbar, with application to titanium-in-quartz (TitaniQ) thermobarometry. Geochim Cosmochim Acta. 2014; 125:196–209.
35. Srijan, Gupta AK. Sustainable material as a column filler in soft clay bed reinforced with encased column: numerical analysis. Scientific Reports. 2025; 15(1):1650.
36. Parisatto M, Turina A, Cruciani G, Mancini L, Peruzzo L, Cesare B. Three-dimensional distribution of primary melt inclusions in garnets by X-ray microtomography. American Mineralogist. 2018; 103(6):911–26.
37. Markussen Ø, Dypvik H, Hammer E, Long H, Hammer Ø. 3D characterization of porosity and authigenic cementation in Triassic conglomerates/arenites in the Edvard Grieg field using 3D micro-CT imaging. Mar Pet Geol. 2019; 99:265–81.
38. Li H, Li H, Wang K, Liu C. Effect of rock composition microstructure and pore characteristics on its rock mechanics properties. Int J Min Sci Technol. 2018; 28(2):303–8.
39. Peng J, Wong LNY, Teh CI. Influence of grain size on strength of polymineralic crystalline rock: new insights from DEM grain-based modeling. J Rock Mech Geotech Eng. 2021; 13(4):755-66. https://doi.org/10.1016/j.jrmge.2021.01.011
40. Bonilla-Jaimes JD, Henao-Martínez JA, Mendoza-Luna C, Castellanos-Alarcón OM, Ríos-Reyes CA. Non-destructive in situ analysis of garnet by combining scanning electron microscopy and X-ray diffraction techniques. Dyna (Medellin). 2016; 83(195):84-92. https://doi.org/10.15446/dyna.v83n195.46360
41. Wahab GMA, Gouda M, Ibrahim G. Study of physical and mechanical properties for some of Eastern Desert dimension marble and granite utilized in building decoration. Ain Shams Eng J. 2019; 10(4):907-15. https://doi.org/10.1016/j.asej.2019.07.003
42. Liu JB, Zhang ZJ, Li B. Microscopic & macroscopic characterizations of Beijing marble as a building material for UNESCO heritage sites: new insights into physico-mechanical property estimation and weathering resistance. Constr Build Mater. 2019; 225:510-25. https://doi.org/10.1016/j.conbuildmat.2019.07.094
43. Whittig LD. X-ray diffraction techniques for mineral identification and mineralogical composition. In: Methods of soil analysis, part 1—physical and mineralogical properties, including statistics of measurement and sampling. Madison, WI: American Society of Agronomy, Soil Science Society of America; 2015; 671-98. https://doi.org/10.2134/agronmonogr9.1.c49
44. Patterson AL. The Scherrer formula for X-ray particle size determination. Phys Rev. 1939; 56(10):978-82. https://doi.org/10.1103/PhysRev.56.978
45. Vishal V, Rizwan M, Mahanta B, Pradhan SP, Singh TN. Temperature effect on the mechanical behavior of shale: implication for shale gas production. Geosyst Geoenv. 2022; 1(4):100078. https://doi.org/10.1016/j.geogeo.2022.100078
46. Braun P, Delage P, Ghabezloo S, Chabot B, Conil N, Vu MN. Inducing tensile failure of claystone through thermal pressurization in a novel triaxial device. Rock Mech Rock Eng. 2022; 55(7):3881-99. https://doi.org/10.1007/s00603-022-02838-3
47. Zou C, Yingying S, Liu K, Cheng Y, Li J. Feasibility of artificial materials in simulating rock failure based on rate-dependent brittleness indexes. Rock Mech Rock Eng. 2022; 55(8):4999-5027. https://doi.org/10.1007/s00603-022-02902-y